

Optimizations of Autonomous Orbit Determination for a Deep-Space CubeSat

Normal Paper

Boris Segret ^{1,3}, Daniel Hestroffer ², Gary Quinsac ³, Marco Agnan ⁴, Jordan Vannitsen ^{4,5}, and Benoît Mosser ³

¹ LabEx ESEP, Paris Observatory, PSL Université Paris, 5 pl.Jules Janssen, 92195 Meudon Cedex, France

² IMCCE, CNRS, Paris Observatory, PSL Université Paris, 77 av. Denfert Rochereau, 75014 Paris, France.

³ LESIA, CNRS, Paris Observatory, PSL Université Paris, 5 pl.Jules Janssen, 92195 Meudon Cedex, France

⁴ ODYSSEUS Space Inc., 6F., No.508, Dongning Rd., East Dist., Tainan City 701, Taiwan (R.O.C.)

⁵ Department of Aeronautics and Astronautics, National Cheng Kung University, Daxue Road, 70101 Tainan City, Taiwan (R.O.C.)

Abstract

Deep-space missions with an autonomous navigation are desirable, but ground navigation and communications are usually preferred. The increasing number of deep-space CubeSats is raising the question again. We have considered a possible on-board orbit determination for a CubeSat with limited optical capabilities and CPU resources. Our results show a global performance of 200 km accuracy at 1- σ in all directions, in less than 1 flying day, in the context of an autonomous cruise from Earth to Mars. We first present a covariance analysis that guides the optimisations and the numeric stability. As we see that a limiting factor is the availability of optical targets, we open the way to an optimised observation strategy, its mathematical context and two notional configurations still in cruise context. Such a strategy still needs to be defined. Further improvements in the architecture of the orbit determination will also allow an application in new contexts, like the proximity operations at an asteroid.

Keywords: CubeSat, Autonomous GNC, Orbit Determination, Deep Space.

Introduction

Future deep-space CubeSats will need to keep their operations at low cost and an autonomous Guidance, Navigation and Control (GNC) would obviously contribute. However, despite early attempts like the DEEP SPACE 1 mission [1], the navigation is mainly performed from the ground and relies on an expensive Deep Space Network (DSN). More propositions to deep space will involve CubeSats (e.g. ESA's Hera, Estonian multi-asteroid touring, Italian LUMIO from Earth-Moon L2). Some autonomy is desirable, at least between successive DSN tracking slots. We have developed an In-Flight Orbit Determination (IFOD) for deep-space CubeSat that relies on optical measurements of foreground objects in front of background stars. The IFOD produces an estimate of the shift of the spacecraft with respect to a reference trajectory stored on-board. The concept was presented in [2] in the context of a cruise from Earth to Mars. The first section reminds the method and presents the latest results. The second section describes the optimisation procedure. Then, the third section introduces the problem of optimised observable targets with notional geometries that could be used to assess in real time the interest of multiple possible targets.

1 – Asynchronous triangulation feeding a Kalman filter

BIRDY-T is a novel technology for an autonomous GNC at nano/micro-satellite scale. It covers IFOD, micro-propulsion and on-board computation of trajectory correction maneuvers. The major requirement for IFOD is to rely on a single small optical device to be successively

pointed to foreground objects in order to provide low resolution measurements of their individual directions (Fig.1).

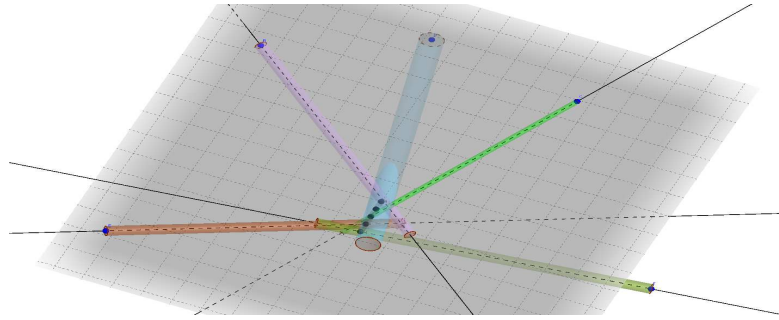


Fig. 1: Asynchronous triangulation. Optical measurements of foreground bodies from successive points of view allowing the triangulation.

As presented in [2], an "Object Tracker" (OT) produces measurements that are processed in an asynchronous triangulation (AT), which feeds a basic linear Kalman Filter (KF). The OT is an optical device with image-processing: the direction of a foreground object of the solar system is determined wrt distant stars in the background. It uses a multiple cross-correlation algorithm that improves the estimated direction, i.e. its variance-covariance matrix (or simply "covariance"). The AT needs a set of 5 measurements and runs a weighted least-squares method (3 measurements being not enough since they are obtained successively and not simultaneously). It yields an estimate of the state vector $[\xi]$ of the moving observer, i.e. the CubeSat: $[\xi]$ is a 9x1-element vector that quantifies the "shifts" in location, velocity and acceleration of the actual trajectory \mathcal{T}_A as compared with a reference trajectory \mathcal{T}_R stored on-board. The state vector is modelled as a random variable Ξ with a normal distribution (\mathcal{N}). Its estimate and its covariance then write:

$$\Xi = \mathcal{N}([\hat{\xi}], (\mathbf{B}^T \cdot \mathbf{W} \cdot \mathbf{B})^{-1}) \quad \text{with} \quad [\xi] = \begin{pmatrix} \delta \vec{r}_{ini} \\ \delta \vec{v}_{ini} \\ \delta \vec{a} \end{pmatrix} \quad (1)$$

$$[\hat{\xi}] = (\mathbf{B}^T \cdot \mathbf{W} \cdot \mathbf{B})^{-1} \cdot (\mathbf{B}^T \cdot \mathbf{W}) \cdot [\mathbf{Y}]$$

$$[\mathbf{B}] = \begin{bmatrix} [\mathbf{B}_j] & dt_j \cdot [\mathbf{B}_j] & \frac{dt_j^2}{2} \cdot [\mathbf{B}_j] \\ \vdots & \vdots & \vdots \end{bmatrix}_{j=1..5} \quad [\mathbf{B}_j] = \frac{1}{\rho_j} \cdot \begin{bmatrix} \sin \lambda_j / \cos \varphi_j & -\cos \lambda_j / \cos \varphi_j & 0 \\ \cos \lambda_j \cdot \sin \varphi_j & \sin \lambda_j \cdot \sin \varphi_j & -\cos \varphi_j \end{bmatrix} \quad (2)$$

where $[\mathbf{Y}]$ is the 10x1 vector of a set of 5 measurements (2 angles per measurement), $[\mathbf{W}]$ is the weight matrix, i.e. the inverse of the 10x10 combined covariance given by the OT, $[\mathbf{B}]$ is the 10x9 Jacobian of the problem, $(\rho_j, \lambda_j, \varphi_j)$ are the coordinates of the j-th foreground object as seen from \mathcal{T}_R at t_j and $dt_j = (t_j - t_{ini})$ with t_{ini} the date of estimate of $[\xi]$. The 5 corresponding successive points of the observer derive from the propagation of initial conditions given by the state vector $[\xi]$. Then the AT is repeated and feeds a linear KF to improve the estimate of $[\xi]$ over the time. The IFOD assumes first that the problem can be linearized due to small parallaxes of the observations between \mathcal{T}_R and \mathcal{T}_A and second that the acceleration difference between \mathcal{T}_R and \mathcal{T}_A can be approximated by a constant vector $\vec{\delta a}$ during any single set of 5 measurements, corresponding to a locally constant gradient (valid in cruise context).

Results are assessed for an Earth-to-Mars cruise scenario with planets Earth, Mars, Jupiter and asteroid Ceres as foreground objects. Two trajectories are simulated: a reference one, \mathcal{T}_R , and an actual one, \mathcal{T}_A , that differs from \mathcal{T}_R after a retrograde ΔV of 1 m/s is applied at the start of the journey (maximum ΔV due to the jettisoning of the CubeSat from the host launcher). \mathcal{T}_A is reconstructed by the IFOD from optical measurements of the foreground objects only, as seen from \mathcal{T}_A , simulated with a Gaussian noise of 0.2" standard deviation (OT requirement).

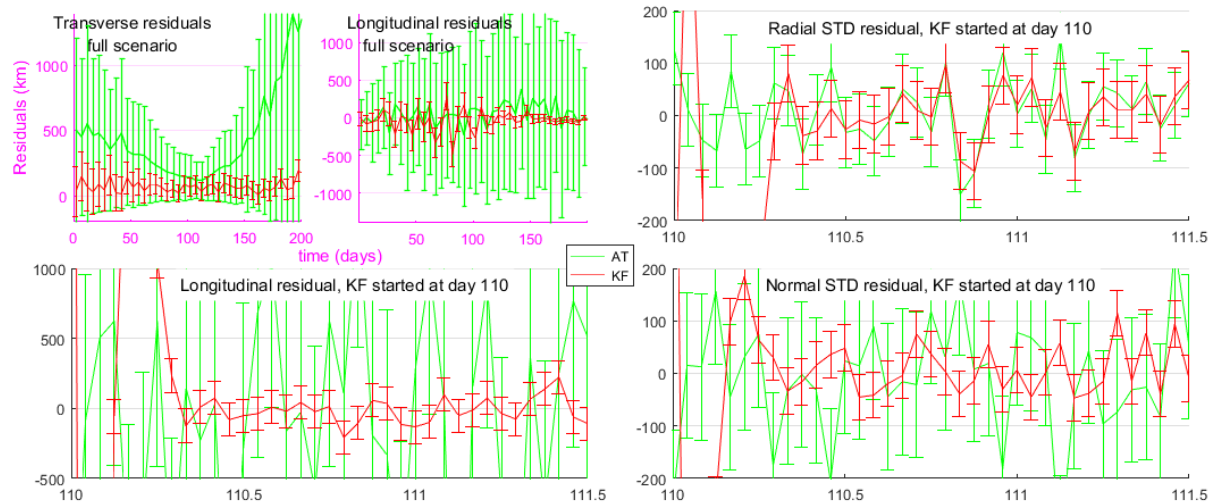


Fig. 2: Residuals for AT and KF, over the full cruise scenario (top-left), detailed KF behavior over 1.5 day when re-started at day 110 (top-right, bottom left & right)

In most cases, with the newest settings and improvements, \mathcal{C}_A is reconstructed transversely with $1\text{-}\sigma$ residuals between -50 and $+150$ km transversely and ± 200 km longitudinally. The convergence of the KF takes less than 1 day, only 0.5 day in the best case when starting at day 110 (Fig.2), with large excursions at start. However some strong residuals are visible, here and there, most likely expressing a non-sufficient system modelling in the linear KF as well as in the linear AT. Also reported in [2], the output accuracy varies proportionally to the optical accuracy, other things being equal, and first depends on the sequence of optical targets.

2 – Analysis tools and numeric settings

A covariance analysis is performed to mitigate the numerical instability and to assess the performance. Most of the settings presented in this section are inspired by Simon, 2006 [3].

Covariance propagation and analysis

Monte-Carlo simulations (MC) were performed in [2] initially but could not provide reliable uncertainties because they do not capture the bias of the method. An IFOD process is run every 5 days of the scenario by re-initializing the KF, then the AT and the KF are monitored for a given number of iterations that allow the convergence of the KF (Fig.3). The covariance of the KF, noted $[P_k^+]$ after the k -th iteration, cannot ensure the convergence by itself, due to the possible bias at start. However, the IFOD process ensures convergence in less than 1 day and a $3\text{-}\sigma$ accuracy better than 600 km in all directions.

We monitor the trace of $[P_k^+]$ as it is a good metric of the overall uncertainties and of the KF behaviour. Indeed $[P_k^+]$ is a square symmetric matrix, then its trace is equal to the sum of its eigenvalues and an orthonormal basis of eigenvectors can transform $[P_k^+]$ into a diagonal matrix of these eigenvalues. Then $\text{tr}([P_k^+])$ is equal to the sum of the variances of independent uncorrelated new random variables built from linear combinations of the parameters of $[u_k^+]$. That is why $\text{tr}([P_k^+])$ is central in Kalman filtering whose core is to minimize $\text{tr}([P_k^+])$ at every iteration and whose goal is to decrease $\text{tr}([P_k^+])$ over successive iterations. The OT produces the covariance of the direction of each observed target resulting from the stars available in the background of the sensor's field of view. The AT produces $[\xi]$ from the problem inversion and also its covariance (see Eq.(1)). The AT then feeds the KF with this "observable" and its covariance, often noted $[v_k]$ and $[Q_k]$ in Kalman filtering, directly taken from the AT:

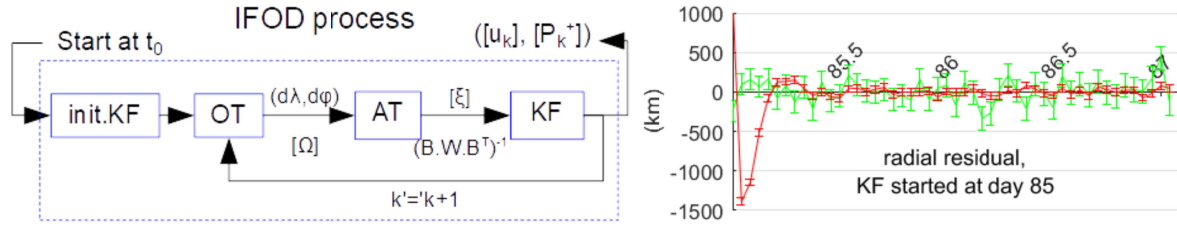


Fig. 3: IFOD process : started at day 85, KF (red) stabilizes after 0.5 days. (AT in green)

$$[v_k] = [\hat{\xi}]_{9 \times 1} \quad \text{and} \quad [Q_k]_{9 \times 9} = (B^T \cdot W \cdot B)^{-1} \quad (3)$$

Compared to [2], this propagation is improved by the transmission of the full state vector and covariance resulting from AT, instead of the position part only (first 3 parameters of $[\hat{\xi}]$). Indeed, the KF is robust against high covariances for $\delta \vec{v}_{ini}$ and $\delta \vec{a}$ in $[\hat{\xi}]$, the additional information even helps the learning stage of the filter to quickly converge.

The traces of the covariance in AT and in KF can be compared to assess the added-value of the KF over time. For AT performance over an entire scenario, however, we chose to show at a given date the average and the standard deviation of AT during each full IFOD process finishing at that date. For a detailed analysis of a given IFOD process, the traces of the covariances of AT and KF are monitored as shown in figure 4. There, the trace for AT is expected to remain flat when the geometry does not evolve (same observation sequences, same uncertainties).

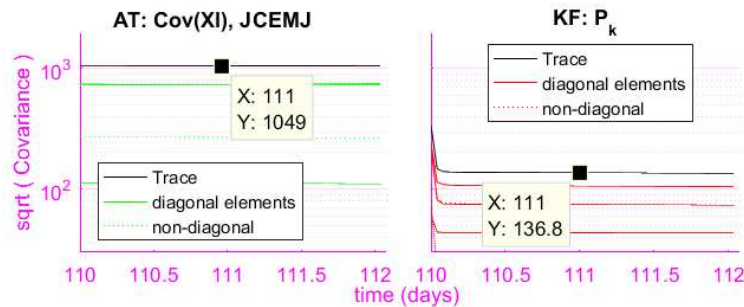


Fig. 4: Square-root of the covariances (in km) during AT (left) and KF (right), at day 110 of the cruise scenario.

Kalman Filter tuning

The numerical stability has been investigated and improved for the IFOD. The ephemerides of planets as well as \mathcal{C}_R and \mathcal{C}_A trajectories' sampling have been taken with sufficient accuracy to avoid effects related to numerical limits. A dimensionless approach has been set up, based on a so-called "condition number" defined as the ratio of the most extreme singular values of a matrix, then $\text{Cov}([\hat{\xi}]_k)$ in AT and P_k in KF are monitored. Also, in order to avoid instabilities after inverting a matrix M that is symmetric by nature, it was first transformed into $(M+M^T)/2$. Eventually, the KF at each IFOD process is initialised with the first $([\hat{\xi}], \text{Cov}([\hat{\xi}]))$ of the process and the model uncertainty for acceleration is set at 0.01 mm/s^2 isotropically.

3 – To a strategy that selects the best next measurement

The observation sequence of targets is a top driver of the IFOD performance: it ensures more or less stability, convergence, accuracy or bias, and reveals a most preferred scheduling to

perform the IFOD. From equation (1), we see that the AT's Jacobian [B] is made of 5 smaller 2x3 blocks [B_j] that link the spherical coordinates (ρ_j, λ_j, φ_j) of the j-th foreground object to the observer's location. A deeper analysis of [B] is beyond the scope of this paper. An attempt at finding the geometry of foreground bodies that best constrains [ξ], i.e. minimising its covariance (B^T.W.B)⁻¹, is to find a set of 5 targets that minimises its trace, or maximizes the trace of its inverse B^T.W.B, that simplifies, after developing, as follows:

$$\text{Max}(\text{tr}(B^T \cdot W \cdot B)) = \text{Max} \left(\sum_{j=1}^5 (1 + dt_j^2 + dt_j^4/2) \cdot \frac{\text{tr}(\Omega_j^{-1})}{\rho_j^2} \right) \text{ if isotropic } \sigma_{\text{opt}} = \text{Max} \left(\sum_{j=1}^5 (1 + dt_j^2 + dt_j^4/2) \cdot \frac{1}{\rho_j^2} \right) \quad (4)$$

where $\text{diag}\{\Omega_j^{-1}\}_{j=1..5} = W$, Ω_j being the covariances given by the Object Tracker. The condition is even simpler with an isotropic optical uncertainty σ_{opt}. This means the longest possible sequence with the closest possible objects, of course within the limits of the modelling, in terms of linearisation (constant δ \vec{a} , small parallaxes) and rank (9 unknowns, 10 equations). No explicit conditions appear for parallaxes.

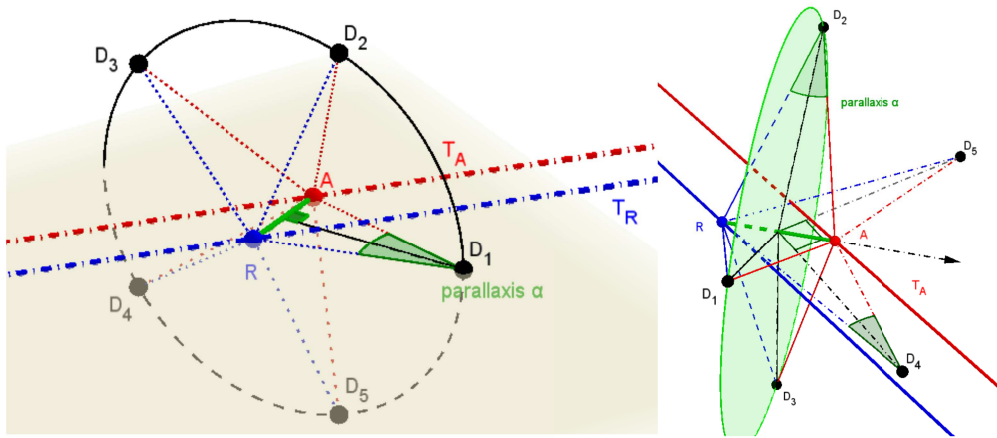


Fig. 5: Construction of notional geometries: wheel-shape (left) ; diabolo-shape (right)

Another attempt is to intuitively define an ideal, purely notional geometry. Thereby, the AT should be better constrained with large (\mathcal{C}_R , \mathcal{C}_A) parallaxes from multiple sectors on the sky. Two geometries are considered (Fig.5): a “wheel-shape” with 5 points regularly spaced on the bisector plan of the segment [R,A], points of \mathcal{C}_R and \mathcal{C}_A , offering a parallax α; a “diabolo-shape” with 3 points on the bisector plan plus 2 points on the orbital plane on \mathcal{C}_A side. The parallaxes α are set to keep the linearisation error much smaller than the optical accuracy σ_{opt} (0.2”=9.7x10⁻⁷ rad). After sin(α) at the 3rd order, we set α = 0.48° (0.0083 rad). The IFOD is run in the Earth-Mars scenario with notional foreground objects defined by these geometries at every time step. Results for the whole scenario are shown in Fig.6. In the “wheel” geometry, the AT is poorly efficient but the KF converges in a few iterations down to a residual of 15±15 km at 3-σ (±5 km, 1-σ). In the “diabolo” geometry, although the AT seems efficient at each IFOD process, with residuals below 25±25 km at 1-σ, both AT and KF converge strictly the same way (estimates and covariances) from typical residuals of 20 km±0.5 km at 1-σ, down to non 0-residual slowly. These results are good insight of the best possible IFOD performances. Thus, there would be an improvement potential due to the geometry by a factor of 10 with the current architecture.

The parallaxes are set to their maximum, typical distances becoming shorter than in a realistic cruise scenario (few 0.01 AUs instead of AUs). Still, these notional geometries were built to keep the modelled system linear, although pushed to the limits. Hence, the unexplained

behaviours may result from a non-constant $\vec{\delta}a$ during AT. These attempts show that an analytical study of [B] is required to properly assess the interest of possible targets.

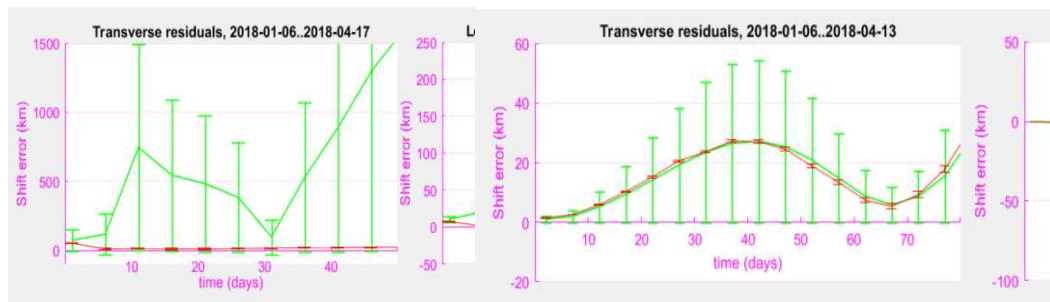


Fig. 6: Residuals for Earth-to-Mars cruise with notional geometries in wheel-shape (left), diabolo-shape (right), AT results in green, KF in red.

Conclusion

We have assumed a possible CubeSat architecture that offers successive optical measurements at low accuracy with limited computation capabilities. The IFOD process shows a fair performance with a simple linear Kalman filter. It converges in 0.5 day and is optimised in a cruise context for its current architecture. The covariance analysis is well adapted while the Monte-Carlo simulations reached some limits and were CPU-consuming. Some improvements are possible: adding new parameters in the state vector, namely a \mathcal{T}_R - \mathcal{T}_A time-shift and even a varying delta-acceleration $\vec{\delta}a$, processing the filter after every measurement instead of every batch of 5 measurements, upgrading to an unscented Kalman filter. These will improve the performance in cruise but also pave the way to use the IFOD in new contexts, like proximity operations at an asteroid.

The observation sequence determines, more than anything, the IFOD performance. An on-the-fly criterion to decide what will be the next best optical targets to observe is desirable but challenging: it requires an analytical investigation of the AT's Jacobian. But it could take advantage of the many asteroids that are available in all directions of the ecliptic plane.

Acknowledgments

This work was funded by the Laboratory of Excellence ESEP in France (ANR-2011-LABX-030) with the Initiative d'excellence PSL (ANR-10-IDEX-0001-02), by the French-Taiwanese program PHC Orchid and was supported in Taiwan by Pr.Miau and Pr.Juang from National Cheng Kung University.

References

1. S. Bhaskaran, J. E. Riedel, and S. P. Synnott, "Autonomous optical navigation for interplanetary missions." Jet Propulsion Laboratory, SPIE AA, Denver CO, 1996.
2. B. Segret, D. Hestroffer, G. Quinsac, M. Agnan, J. Vannitsen, and B. Mosser, "In-Flight Orbit Determination for a Deep Space CubeSat," in *IEEE Aerospace Conference*, 2018.
3. D. Simon, *Optimal State Estimation*, First Edit. WILEY-INTERSCIENCE, 2006.